Journal of Solid State Chemistry 182 (2009) 1861–1866

Contents lists available at ScienceDirect

Journal of Solid State Chemistry

journal homepage: www.elsevier.com/locate/jssc

Synthesis and characterization of the new uranium yttrium oxysulfide $UY_4O_3S_5$

Geng Bang Jin [a], Eun Sang Choi [b], Daniel M. Wells [a], James A. Ibers [a,*]

[a] Department of Chemistry, Northwestern University, 2145 Sheridan Road, Evanston, IL 60208-3113, USA
[b] Department of Physics and National High Magnetic Field Laboratory, Florida State University, Tallahassee, FL 32310, USA

ARTICLE INFO

Article history:
Received 16 January 2009
Received in revised form
11 April 2009
Accepted 20 April 2009
Available online 3 May 2009

Keywords:
Uranium yttrium oxysulfide
X-ray crystal structure
Paramagnetic
Band gap
Activation energy

ABSTRACT

Red needles of $UY_4O_3S_5$ have been synthesized by the solid-state reaction at 1273 K of UOS and Y_2S_3 with Sb_2S_3 as a flux. $UY_4O_3S_5$ adopts a three-dimensional structure that contains five crystallographically unique heavy-atom positions. U and Y atoms disorder on one eight-coordinate metal position bonded to four O atoms and four S atoms and two seven-coordinate metal positions bonded to three O atoms and four S atoms. Another eight-coordinate metal position with two O and six S atoms and one six-coordinate metal position with six S atoms are exclusively occupied by Y atoms. $UY_4O_3S_5$ is a modified Curie–Weiss paramagnet between 1.8 and 300 K. Its effective magnetic moment is estimated to be 3.3(2) μ_B. $UY_4O_3S_5$ has a band gap of 1.95 eV. The electrical resistivity along the [010] direction of a single crystal shows Arrhenius-type thermal activation with an activation energy of 0.2 eV.

1. Introduction

Both solid-state uranium oxides and sulfides exhibit rich chemistries [1,2]. Even simple binary compounds exist in diverse stoichiometries and structures [1]. In contrast, solid-state uranium oxysulfides are rare. To our knowledge UOS [3], $U_2LnO_2S_3$ (Ln = Gd–Lu, Y) [4,5], $U_4LuO_4S_5$ [6], $Cs_4(UO_2)(S_2)_3$ [7], $Na_4(UO_2)(S_2)_3 \cdot Na_2S_3$ [7], and $Na_4(UO_2)Cu_2S_4$ [8] are the only uranium oxysulfides whose structures are known from single-crystal diffraction studies. UOS [3], $U_2LnO_2S_3$ (Ln = Gd–Lu, Y) [4,5], and $U_4LuO_4S_5$ [6] possess no U=O double bonds. $Cs_4(UO_2)(S_2)_3$ [7], $Na_4(UO_2)(S_2)_3 \cdot Na_2S_3$ [7], and $Na_4(UO_2)Cu_2S_4$ [8] contain uranyl (UO_2^{2+}) cations, which have U=O double bonds.

The high stability of uranium oxides makes difficult the synthesis of new uranium oxysulfides. For the above uranium rare-earth oxysulfides high reaction temperatures (> 1573 K) and UOS as a starting material were needed. For those containing U=O double bonds the use of highly stable UO_2^{2+} cations as building units was necessary.

Both $U_2LnO_2S_3$ [4–5] and $U_4LuO_4S_5$ [6] adopt interesting layered structures where (UOS) and (LnS) form individual layers. On the basis of charge balance and crystallographic data the formal oxidation states of U are +3.5 in $U_2LnO_2S_3$ and +3.5/+4.0 in $U_4LuO_4S_5$. Because we thought an average oxidation state of +3.5 for U to be unusual we began a reinvestigation of those compounds. In the course of that work we discovered the new uranium yttrium oxysulfide, $UY_4O_3S_5$. We report its synthesis, structure, and optical and magnetic properties here.

2. Experimental

2.1. Synthesis

UO_2 (Strem Chemicals, 99.8%), Y_2S_3 (Alfa-Aesar, 99.9%), S (Alfa-Aesar, 99.99%), and Sb (Aldrich, 99.5%) were used as received. Sb_2S_3 was prepared from the direct reaction of the elements in a sealed fused-silica tube at 1123 K. UOS was prepared by a solid–gas reaction among UO_2, S, and C at 1213 K [9]. The purities of Y_2S_3, UOS, and Sb_2S_3 were confirmed by powder X-ray diffraction measurements.

Before being loaded into a fused-silica tube 0.161 g (0.563 mmol) of UOS and 0.039 g (0.14 mmol) of Y_2S_3 were thoroughly ground together. The tube was flame sealed under vacuum and heated in a computer-controlled furnace at 1273 K for 6 d. The resultant powder was ground again with 0.100 g of Sb_2S_3 flux and the mixture was loaded into a fused-silica tube that was then vacuum sealed. The reaction mixture was heated to 1273 K in 40 h, kept at 1273 K for 8 d, cooled to 773 K in 8 d, and then cooled to 298 K in 8 h. The reaction products, as deduced from diffraction measurements, included long red needles of $UY_4O_3S_5$ and dark-red square plates of $UY_2O_2S_3$ [10], which was previously

* Corresponding author. Fax: +1 847 491 2976.
E-mail address: ibers@chem.northwestern.edu (J.A. Ibers).

0022-4596/$ - see front matter © 2009 Elsevier Inc. All rights reserved.
doi:10.1016/j.jssc.2009.04.023

characterized as $U_2YO_2S_3$ [4]. Both compounds are stable in air. The yields of $UY_4O_3S_5$ and $UY_2O_2S_3$ were about 10% and 5%, respectively, based on Y. Also in the tube were unreacted black UOS powder, orange Y_2S_3 crystals, and black Sb_2S_3 crystals.

2.2. Analyses

Selected single crystals of $UY_4O_3S_5$ were examined with an EDX-equipped Hitachi S-3400 SEM. The presence of U, Y, and S was confirmed. No Sb was detected. O could not be detected because its emission line is below the lower limit of the instrument.

An ICP measurement to quantify the U:Y ratio was conducted on a sample of about 0.5 mg of single crystals of $UY_4O_3S_5$. The red needles were carefully selected and cleaned before being dissolved in 0.72 mL 68–70% HNO_3 solution. The solution was diluted to 10 mL and analyzed on a Varian VISTA-MPX instrument. Five U and Y standard solutions were used. The ratio U:Y was determined to be 0.28(1).

2.3. Structure determination

Single-crystal X-ray diffraction data for $UY_4O_3S_5$ were collected with the use of graphite-monochromatized Mo$K\alpha$ radiation ($\lambda = 0.71073$ Å) at 100 K on a Bruker APEX2 diffractometer [11]. The crystal-to-detector distance was 5.023 cm. Crystal decay was monitored by recollecting 50 initial frames at the end of the data collection. Data were collected by a scan of 0.3° in ω in groups of 606 frames at φ settings of 0°, 90°, 180°, and 270°. The exposure time was 30 s/frame. The collection of intensity data was carried out with the program APEX2 [11]. Cell refinement and data reduction were carried out with the use of the program APEX2

Table 1
Least-squares refinements for $UY_4O_3S_5$.

Formula	R (F)[a]	R_w (F^2)[a]	Details
$U_{0.79(1)}Y_{4.21(1)}O_3S_5$	0.0177	0.0459	anisotropic; no restraints
$UY_4O_3S_5$	0.0238	0.0794	anisotropic; restrained[b]
$U_{0.79(1)}Y_{4.21(1)}O_3S_5$	0.0248	0.0719	isotropic; no restraints
$UY_4O_3S_5$[d]	0.0293	0.1005	isotropic; restrained[c]

[a] Defined in Table 2.
[b] Non-positive definite displacement ellipsoid for atom Y(5).
[c] Chosen refinement.
[d] The U occupancies are 0.418(2), 0.400(2), and 0.182(2) at positions $M(1)$, $M(2)$, and $M(3)$, respectively.

Table 2
Crystal data and structure refinements for $UY_4O_3S_5$.

Fw	801.97
Space group	*Pnma*
Z	4
a (Å)	13.9193 (3)
b (Å)	3.8438 (1)
c (Å)	18.5114 (4)
V (Å^3)	990.42 (4)
T (K)	100 (2)
λ (Å)	0.71073
ρ_c (g cm^{-3})	5.378
μ (cm^{-1})	404.91
$R(F)$[a]	0.0293
$R_w(F^2)$[b]	0.1005

[a] $R(F) = \sum ||F_o| - |F_c|| / \sum |F_o|$ for $F_o^2 > 2\sigma(F_o^2)$.
[b] $R_w(F_o^2) = \{\sum[w(F_o^2 - F_c^2)^2] / \sum wF_o^4\}^{1/2} \cdot w^{-1} = \sigma^2(F_o^2) + (0.0411 \times F_o^2)^2$. for $F_o^2 \geq 0$; $w^{-1} = \sigma^2(F_o^2)$ for $F_o^2 < 0$.

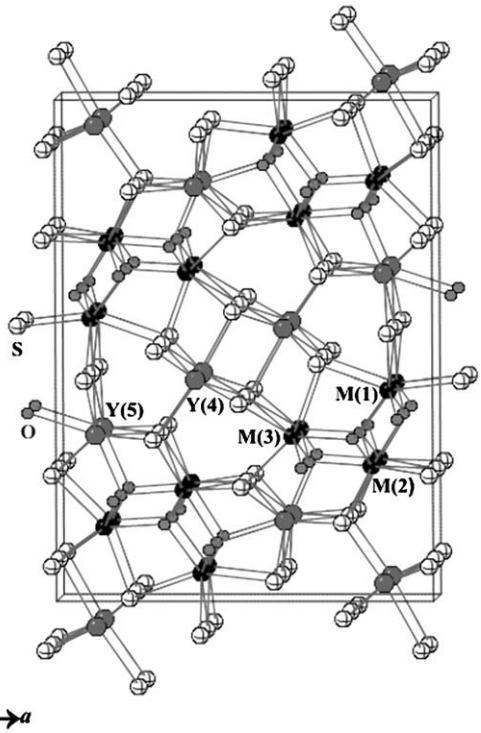

Fig. 1. View down [010] of the three-dimensional structure of $UY_4O_3S_5$.

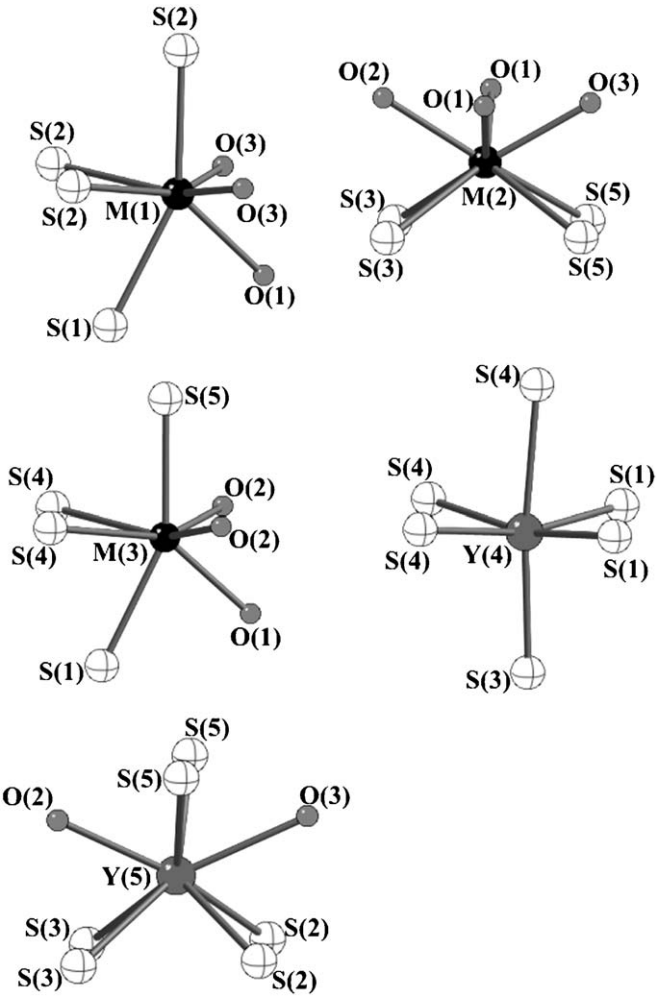

Fig. 2. Illustrations of coordination environments for the five metal positions in $UY_4O_3S_5$.

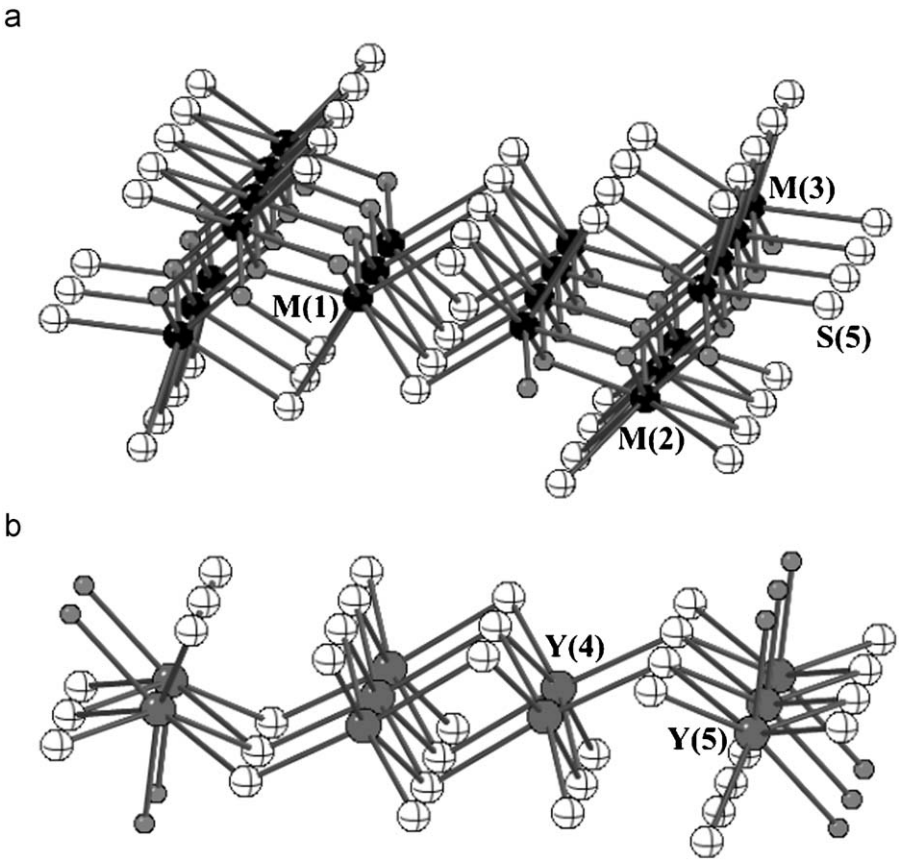

Fig. 3. (a) Depiction of an individual slab formed by $(U/Y)O_XS_Y$ polyhedral along the [010] direction and (b) depiction of the connectivities among two single $Y(4)O_2S_6$ chains and one double $Y(5)S_6$ octahedral chain down the [010] direction.

[11]. A Leitz microscope equipped with a calibrated traveling micrometer eyepiece was employed to measure accurately the crystal dimensions. Face-indexed absorption corrections were performed numerically with the use of the program XPREP [12]. Then the program SADABS [13] was employed to make incident beam and decay corrections.

The structure was solved with the direct-methods program SHELXS and refined with the full-matrix least-squares program SHELXL [12]. In the asymmetric unit there are five heavy-atom positions (*M*) and eight light-atom positions. All positions have site symmetry *m*. The latter could readily be assigned to three O and five S atoms. However, the assignment of the five *M* atoms was not straightforward. From the peak heights, disorder of U and Y was suspected. Note that the effective ionic radius of U^{4+} is only 0.01 Å smaller than that of Y^{3+} [14]. Disorder of U and Y was introduced at each of the five *M* positions with individual occupancies but with the same positional and isotropic displacement parameters assigned. This refinement showed that U and Y disorder at the *M*(1), *M*(2), and *M*(3) positions but only Y atoms occupy the *M*(4) and *M*(5) positions. Next, this model was refined anisotropically in the normal manner. This refinement led to a formula that requires the average oxidation state of U to be +4.3. This refinement was modified to restrain the combined occupancies at the *M*(1), *M*(2), and *M*(3) positions so that charge balance with U^{4+} and Y^{3+} is achieved. This refinement resulted in a non-positive displacement ellipsoid for atom Y(5). Finally, the corresponding isotropic refinements were carried out. The unrestrained refinement requires the average oxidation state of U to be +4.3. The restrained isotropic refinement has no problems.

Table 1 gives some details on these four refinements. All four give satisfactory *R* indices. In particular, the differences between the restrained and unrestrained refinements are small. The structural model being refined is a complicated one, with variable disorder in three of the five heavy-atom positions. The material is a heavy absorber with a linear absorption coefficient of over 400 cm^{-1}. Even in the best of circumstances, and this does not apply here, the use of single-crystal X-ray diffraction data to "determine" compositions is ill-advised [15]. For this reason we have no faith in the formulas deduced from the unrestrained refinements. The restrained anisotropic refinement results in the displacement ellipsoid of atom Y(5) being non-positive definite. Thus we chose the restrained isotropic model (formula $UY_4O_3S_5$), as the one to be discussed here. The ICP analysis leads to the formula $U_{1.1}Y_{3.9}O_3S_5$.

Table 3
Selected interatomic distances (Å) for $UY_4O_3S_5$.

U(1)/Y(1)–O(1)	2.25(1)	U(3)/Y(3)–(1)	2.79(1)
U(1)/Y(1)–O(3) × 2	2.20(1)	U(3)/Y(3)–S(4) × 2	2.95(1)
U(1)/Y(1)–S(1)	2.78(1)	U(3)/Y(3)–S(5)	2.71(1)
U(1)/Y(1)–S(2) × 2	2.91(1)	Y(4)–S(1) × 2	2.637(1)
U(1)/Y(1)–S(2)	2.71(1)	Y(4)–S(3)	2.710(2)
U(2)/Y(2)–O(1) × 2	2.29(1)	Y(4)–S(4) × 2	2.734(1)
U(2)/Y(2)–O(2)	2.30(1)	Y(4)–S(4)	2.861(2)
U(2)/Y(2)–O(3)	2.29(1)	Y(5)–O(2)	2.405(5)
U(2)/Y(2)–S(3) × 2	2.93(1)	Y(5)–O(3)	2.657(5)
U(2)/Y(2)–S(5) × 2	2.97(1)	Y(5)–S(2) × 2	2.852(2)
U(3)/Y(3)–O(1)	2.24(1)	Y(5)–S(3) × 2	2.975(2)
U(3)/Y(3)–O(2) × 2	2.25(1)	Y(5)–S(5) × 2	2.777(1)

U/Y–O and U/Y–S interatomic distances are truncated to two decimal places because of the U/Y disorder. The difference between effective ionic radii of U^{4+} and Y^{3+} is 0.01 Å [14].

The program STRUCTURE TIDY [16] was used to standardize the positional parameters. Additional experimental details are given in Table 2 and the Supporting material.

2.4. Powder X-ray diffraction measurement

Powder X-ray diffraction patterns were collected with a Rigaku Geigerflex powder X-ray diffractometer with the use of Cu$K\alpha$ radiation ($\lambda = 1.54056$ Å).

2.5. Magnetic susceptibility measurement

In order to get at least a minimal sample for magnetic measurements a needle cluster of $UY_4O_3S_5$ weighing 6.16 mg was isolated. Unfortunately, this cluster was contaminated with a layer of black Sb_2S_3 crystals that could not be removed manually without losing most of the sample. Note that Sb_2S_3 is diamagnetic. The needle cluster was loaded into a polycarbonate capsule holder that was then placed in a Quantum Design MPMS instrument. DC susceptibility measurements were made under zero-field-cooled conditions with an applied field of 0.1 T.

After the magnetic measurements were completed the needle cluster was ground and examined by powder X-ray diffraction methods. The sample was found to comprise only $UY_4O_3S_5$ and Sb_2S_3. From an analysis of peak heights and areas the masses of $UY_4O_3S_5$ and Sb_2S_3 were estimated to be 2.76 and 3.40 mg, respectively.

2.6. Single-crystal optical measurement

A clean single crystal of $UY_4O_3S_5$ was selected and placed under light mineral oil on a glass slide. The absorption data were collected from 380 (3.27 eV) to 900 nm (1.38 eV) at 293 K with a Hitachi U6000 microscopic FT spectrophotometer. The absorbance of oil and glass was subtracted as a background.

2.7. Single crystal resistivity

The electrical resistivity of a single crystal of $UY_4O_3S_5$ was measured along [010] between 243 and 300 K by standard two-probe ac methods with the use of a HP 3456A digital voltmeter while the temperature was controlled within a Quantum Design PPMS instrument. A crystal, 1.42 mm in length with a cross-sectional area of 0.00090 mm^2, was mounted with four leads constructed of 15 μm diameter Cu wire and 8 μm diameter graphite fibers, and attached with Dow 4929N silver paint. The resistance was too high to be measured on the Quantum Design PPMS; however, the resistance between the two closest leads, 0.14 mm apart, could be measured on the voltmeter. Attempts at measurements below 243 K were unsuccessful. As the lowest resistance measured was of the order of $10^8\,\Omega$, the resistance of the leads may be neglected.

3. Results and discussion

3.1. Synthesis

During attempts to synthesize $U_2YO_2S_3$, red needles of $UY_4O_3S_5$ were obtained in about 10 wt% yield by the solid-state reaction at 1273 K of UOS and Y_2S_3 with Sb_2S_3 as a flux. Numerous variations in starting materials, temperature regimes, and stoichiometries did not improve the yield.

3.2. Structure

$UY_4O_3S_5$ crystallizes in a complex three-dimensional structure, as shown in Fig. 1. There are five crystallographically independent metal positions in the cell. As discussed above, U and Y atoms disorder at the $M(1)$, $M(2)$, and $M(3)$ positions but only Y atoms occupy the $M(4)$ and $M(5)$ positions. The coordination environments for each metal position are displayed in Fig. 2. Both the U(1)/Y(1) and U(3)/Y(3) atoms are coordinated to three O and four S atoms in a seven-octahedron. Atom U(2)/Y(2) is surrounded by four O and four S atoms in a square-antiprismatic arrangement that has been seen in $U_2LnO_2S_3$ (Ln = Gd-Lu, Y) [4–5] and $U_4LuO_4S_5$ [6]. Atom Y(4) is octahedrally coordinated by six S atoms. Atom Y(5) is connected to two O and six S atoms in a bicapped trigonal prism.

The eight-coordinated polyhedra face share and the six- or seven-coordinated polyhedra edge share along the b axis to form one-dimensional chains. $(U/Y)O_XS_Y$ polyhedral chains share edges in the ac plane to form slabs (Fig. 3a). These slabs are further connected at S(5) positions with each other to construct the three-dimensional structure. The space between $(U/Y)O_XS_Y$ slabs is filled by two single $Y(4)O_2S_6$ chains and one double $Y(5)S_6$ octahedral chain (Fig. 3b).

Selected interatomic distances for $UY_4O_3S_5$ are listed in Table 3. Examples with U and Y atoms adopting coordination environments similar to those of $M(1)$, $M(2)$, $M(3)$, and Y(5) are very rare. U/Y–O distances range from 2.20(1) to 2.30(1) Å; these are shorter

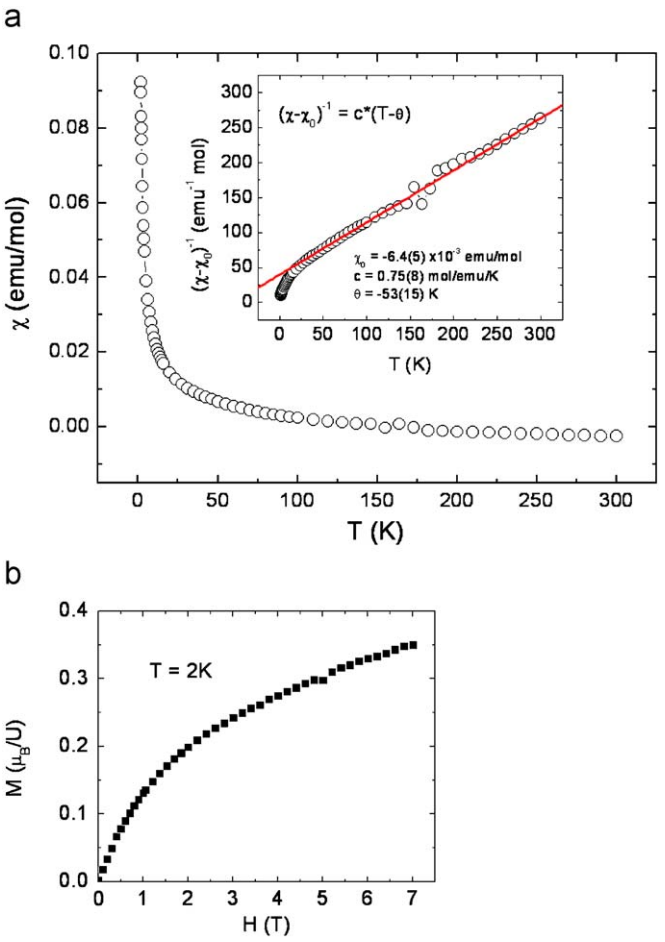

Fig. 4. (a) DC magnetic susceptibility of $UY_4O_3S_5$. The inset shows $(\chi-\chi_0)^{-1}$ versus temperature and the best fit of the modified inverse Curie–Weiss equation and (b) magnetization data at 2 K.

than that of 2.35 Å for nine-coordinate U^{4+} cations in UOS [3]. The U/Y–S distances of 2.71(1) to 2.97(1) Å in $UY_4O_3S_5$ and 2.890 to 2.935 Å in UOS agree. Y(4)–S distances range from 2.637(1) to 2.861(2) Å, close to those of 2.626(3)–2.819(3) Å found for octahedral Y^{3+} cations in δ-Y_2S_3 [17]. As expected, for the eight-coordinated Y(5) atom the Y–O (2.405(5)–2.657(5) Å) and Y–S (2.777(1)–2.975(2) Å) distances are somewhat longer than those of 2.249–2.276 Å and 2.732–2.934 Å for seven-coordinate Y^{3+} cations in Y_2OS_2 [17].

3.3. Magnetic susceptibility

Fig. 4a shows the magnetic susceptibility of the $UY_4O_3S_5/Sb_2S_3$ needle cluster between 1.8 and 300 K. The susceptibility shows no magnetic ordering. At high temperatures, the susceptibility becomes negative owing to the diamagnetic Sb_2S_3 phase. By using the mass of $UY_4O_3S_5$ estimated from the powder diffraction analysis and using the modified inverse Curie–Weiss fitting between 50 and 300 K, we estimate the effective moment to be about 3.3(2) μ_B, which is slightly smaller than a theoretical value 3.6 μ_B/U^{4+} but is similar to those of other U^{4+} compounds [18]. The negative temperature independent term (χ_0) represents the diamagnetic contribution from the Sb_2S_3 phase and the sample holder. At lower temperatures, a deviation from the modified Curie–Weiss behavior occurs owing to the crystalline electric field. The fitted Weiss temperature (θ) of about −53(15) K may result from antiferromagnetic exchange coupling between U atoms. The magnetization data at 2 K after the diamagnetic background was subtracted are shown in Fig. 4b. Although the moment is far from saturation under a 7 T field, by extrapolation to zero of M versus $1/H$ we estimate the saturation moment to be 0.50(3) μ_B/U^{4+}.

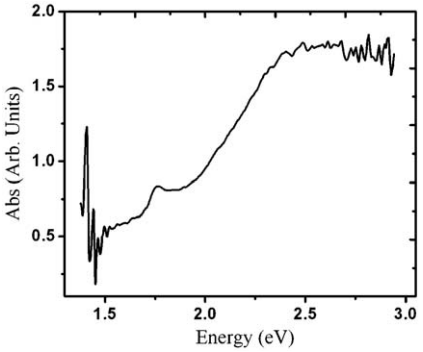

Fig. 5. Single-crystal absorption spectrum of $UY_4O_3S_5$.

3.4. Optical properties

The single-crystal absorption spectrum of $UY_4O_3S_5$ is shown in Fig. 5. By extrapolation the optical band gap of $UY_4O_3S_5$ is determined to be 1.95 eV. The gradual slope of the optical absorption edge and the tail below the edge suggest an indirect transition. The observed fine structures between 1.40 and 1.50 eV result from *f*–*f* transitions within U atoms.

3.5. Single crystal resistivity

The temperature dependent electrical resistivity along the [010] direction in $UY_4O_3S_5$ between 243 and 300 K is displayed in Fig. 6. The resistivity decreases with increasing temperature in accordance with semiconductor-like conduction. The resistivity at 298 K is 75 kΩ cm. Below 243 K the resistance ρ in the [010] direction exceeds 10^6 kΩ, the limit that could be measured. The plot of ln ρ vs. $1/T$ can be fit to a simple Arrhenius-type thermal activation equation, $\rho = \rho_0 \exp -(E_a/k_BT)$ with the estimated activation energy E_a equal to 0.2 eV. The optically determined band gap E_g of 1.95 eV is much larger. Therefore, the material is not an intrinsic semiconductor where one expects $E_a = \frac{1}{2}E_g$ [19].

Supporting material

The crystallographic file in CIF format for $UY_4O_3S_5$ has been deposited with FIZ. Karlsruhe as CSD number 420233. It may be obtained free of charge by contacting FIZ Karlsruhe at +497247808 666 (fax) or crysdata@fiz-karlsruhe.de (e-mail).

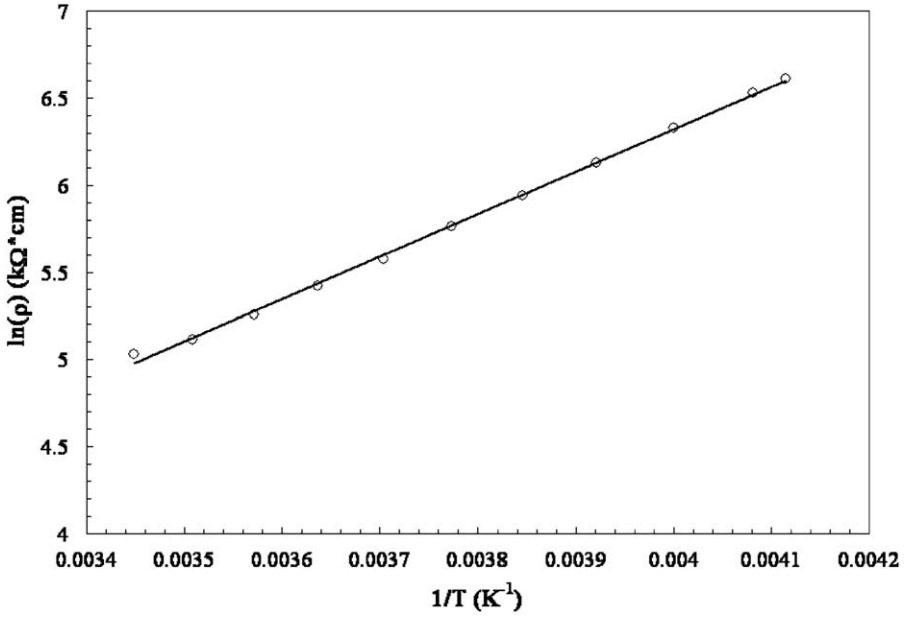

Fig. 6. Temperature dependent electrical resistivity along the [100] direction in $UY_4O_3S_5$.

Acknowledgments

We thank Dr. Christos Malliakas and Prof. Mercouri G. Kanatzidis for help with the use of their single-crystal absorption spectrometer. This research was supported by the US Department of Energy, Basic Energy Sciences Grant ER-15522. Resistivity measurements were collected at the Northwestern University Materials Research Science and Engineering Center, Magnet and Low Temperature Facility supported by the National Science Foundation (DMR05–20513). The NHMFL is supported by NSF through Grant No. NSF-DMR-0084173 and the State of Florida.

Appendix A. Supplementary material

Supplementary data associated with this article can be found in the online version at doi:10.1016/j.jssc.2009.04.023.

References

[1] I. Grenthe, J. Drozdzynski, T. Fujino, E.C. Buck, T.E. Albrecht-Schmitt, S.F. Wolf, Uranium, in: L.R. Morss, N.M. Edelstein, J. Fuger (Eds.), The Chemistry of the Actinide and Transactinide Elements, vol. 1, third ed., Springer, Dordrecht, 2006, pp. 253–698.
[2] A.A. Narducci, J.A. Ibers, Chem. Mater. 10 (1998) 2811–2823.
[3] G.V. Ellert, G.M. Kuz'micheva, A.A. Eliseev, V.K. Slovyanskikh, S.P. Morozov, Russ. J. Inorg. Chem. (Transl. of Zh. Neorg. Khim.) 19 (1974) 1548–1551.
[4] M. Guittard, T. Vovan, M. Julien-Pouzol, S. Jaulmes, P. Laruelle, J. Flahaut, Z. Anorg. Allg. Chem. 540/541 (1986) 59–66.
[5] S. Jaulmes, M. Julien-Pouzol, M. Guittard, T. Vovan, P. Laruelle, J. Flahaut, Acta Crystallogr. Sect. C Cryst. Struct. Commun. 42 (1986) 1109–1111.
[6] S. Jaulmes, M. Julien-Pouzol, J. Dugué, P. Laurelle, T. Vovan, M. Guittard, Acta Crystallogr. Sect. C Cryst. Struct. Commun. 46 (1990) 1205–1207.
[7] A.C. Sutorik, M.G. Kanatzidis, Polyhedron 16 (1997) 3921–3927.
[8] A.C. Sutorik, M.G. Kanatzidis, J. Am. Chem. Soc. 119 (1997) 7901–7902.
[9] R.C. Larroque, M. Beauvy, J. Less-Common Met. 121 (1986) 487–496.
[10] G.B. Jin, E.S. Choi, J.A. Ibers J. Solid State Chem., submitted.
[11] Bruker, APEX2 version 2008.6-1 and SAINT version 7.34a Data Collection and Processing Software, Bruker Analytical X-ray Instruments, Inc. Madison, WI, USA, 2006.
[12] G.M. Sheldrick, Acta Crystallogr. Sect. A Found. Crystallogr. 64 (2008) 112–122.
[13] G.M. Sheldrick, SADABS version 2008/1, Bruker Analytical X-ray Instruments, Inc., Madison, WI, USA.
[14] R.D. Shannon, Acta Crystallogr. Sect. A Cryst. Phys. Diffr. Theor. Gen. Crystallogr. 32 (1976) 751–767.
[15] Y.V. Mironov, J.A. Cody, T.E. Albrecht-Schmitt, J.A. Ibers, J. Am. Chem. Soc. 119 (1997) 493–498.
[16] L.M. Gelato, E. Parthé, J. Appl. Crystallogr. 20 (1987) 139–143.
[17] T. Schleid, Eur. J. Solid State Inorg. Chem. 29 (1992) 1015–1028.
[18] H. Noël, R. Troc, J. Solid State Chem. 27 (1979) 123–135.
[19] C. Kittel, Introduction to Solid State Physics, seventh ed., Wiley, New York, 1996.